Analysis, Optimization, Fabrication and Test of Composite Shells with Embedded Viscoelastic Layers

Allen J. Bronowicki[1]
Henry P. Diaz [2]

TRW Space & Technology Group
Redondo Beach CA 90278

March 10, 1989

Abstract

Large space structures for the 90's and beyond require a combination of high stiffness, light weight and vibration attenuation not heretofore available. Advanced composites offer high stiffness while viscoelastic materials offer vibration attenuation. Both are light in weight. This paper describes finite analysis tools, and design and fabrication concepts which makes a marriage of these two material technologies feasible.

A special purpose finite element based on closed form solutions in membrane cylindrical shells is derived. Two concentric composite shells with an embedded viscoelastic layer can be analyzed with one element. Complex ply arrangements such as the Alternating Ply Concept (patent pending) can be analyzed with as few as five elements.

The analysis code was tied to an optimization package. A material figure of merit based on specific modulus weighted by a power of loss factor is optimized. A tube employing the Alternating Ply Concept, was designed using the code and fabricated. Greater than 5.5% damping was achieved across a 50° F temperature range using a relatively low loss factor silicone damping material.

[1]Head, Analytic Methods Section
[2]Member of the Technical Staff, Dynamics Department

1 Introduction

Currently planned large space structures must be agile and precise. Agility involves the ability to maneuver rapidly and regain shape and pointing stability in minimum time. Precision involves the ability to maintain shape and pointing stability in the presence of dynamic and thermal disturbances. Both agility and precision can be enhanced by the use of structural concepts and materials which maximize stiffness and damping within constraints on total system mass.

Advanced composite materials can offer very high stiffness to weight ratios. This was verified in recent tests at TRW on Pitch-130 graphite epoxy in a unidirectional layup [1]. A tensile modulus of 80.6 million psi was achieved in a 60% fiber volume laminate. At a density of 0.065 lb/in^3, this gives a specific modulus of 1.24 $\times 10^9$ inches. Near zero coefficient of thermal expansion (CTE) in a single direction can be achieved in graphite epoxy laminates through tailoring of ply angles, although this degrades specific modulus in the loading direction. Metal matrix composites (MMC) employing the same fiber material as an organic matrix composite will achieve somewhat lower specific stiffness since only a 50% fiber volume can be achieved in practice. MMC's can claim a distinct advantage over organic matrices in applications where near zero CTE in a single direction is desired, since no off angle plies will be required.

Viscoelastic materials (VEM) offer high energy absorption capability, again with low weight. For instance, an organic polymer such as the 3M ISD-110 material at room temperature can provide a loss factor, η, above 1.0 across several decades of frequency [2]. The density of this material is only 0.03 lb/in^3.

The blending of advanced composites with viscoelastic damping materials offers the most likely means of meeting the dynamics requirements on precision and agility. If applied on truss structures, it will be necessary to devise a means of damping extensional motions in a member. The common practice in damping technology is to apply a continuous constraining layer to a base structure. This succeeds in damping flexural motions but not extensional motions. By segmenting the constraining layer periodically in the direction of loading, both extensional and flexural motions can be damped [3]. A segmentation length which maximizes loss factor can be derived in closed form [4]. This optimum length is 3.278 times the shear lag decay length commonly employed in the design of bonded joints. Graphite epoxy tubes with a viscoelastic damping layer and a unidirectional (all 0° plies) segmented constraining layer cocured on top have been fabricated at TRW [5]. The advantage of cocuring the VEM and constraining layer is the void free bond one can create. Application of a precured 0° constraining layer to a cylindrical surface is very difficult. Application of precured angle plies would not be possible at all. Even though it is difficult to cocure a viscoelastic material with a transition temperature below the epoxy cure temperature, the performance and fabrication advantages make the effort worthwhile.

The practical limit to damping using the segmented constraining layer approach is η = 0.1-0.12, or ζ = 5-6%. One can increase damping using constraining layers much stiffer

than the base tube, but a figure of merit normalized by weight will begin to diminish. This practical limit on damping motivated the research described in this paper. It was apparent that more complex ply layups would be necessary to increase the strain energy induced in the VEM. This necessitated the development of new analysis and design tools as described in the ensuing sections.

2 Derivation of Finite Element for Concentric Shells Enclosing a Viscoelastic Medium

The analysis of constrained layer viscoelastic treatments for cylindrical tubes can become exceedingly complex when the properties of the tube, the constraining layer and the viscoelastic medium vary along the length of the tube. In many design concepts, such as TRW's proprietary Alternating Ply Concept, it is difficult to decide which is the base structure and which is the constraining layer. Material properties and thickness can vary considerably both along the length of the tube and on either side of the viscoelastic layer. Closed form solutions become inappropriate in this case.

Standard finite element analysis using plate and solid elements is also difficult in complex situations on curved surfaces with thin viscoelastic layers. Up to thousands of elements can be required to analyze one structural component in a larger structure.

The path taken here has been to develop a semi-analytical finite element based on closed form solutions for a pair of concentric cylindrical membrane shells surrounding a uniform elastic medium in a state of axisymmetric deformation. The viscoelastic nature of the problem is handled quite simply by assuming that motions are harmonic in time at a given frequency. This allows a complex modulus valid for that operating frequency to be employed. The resultant calculations are performed in complex arithmetic. The magnitude of the displacements for a given force input indicates overall tube stiffness. Tube damping or loss factor can be derived from the tangent of the displacement, which is indicative of phase of the displacement with respect to the force.

The semi-analytic solution allows a very coarse grid to be employed along the length of the tube. All the shear lag effects are modeled exactly. Only a few elements are required, typically between one and six. This makes computation time extremely short, allowing optimization algorithms to be employed inexpensively.

By analogy to the Bernoulli-Euler hypothesis, the results of the axial analysis can be applied to beam bending performance in many cases. This has been found to work quite well in test and in comparison to ordinary FEM analysis in most cases, particularly when constraining layer shear stiffness is low, or if constraining layer segments are short.

2.1 Membrane Cylinder Constitutive Equations

2 CONCENTRIC SHELL FINITE ELEMENT DERIVATION

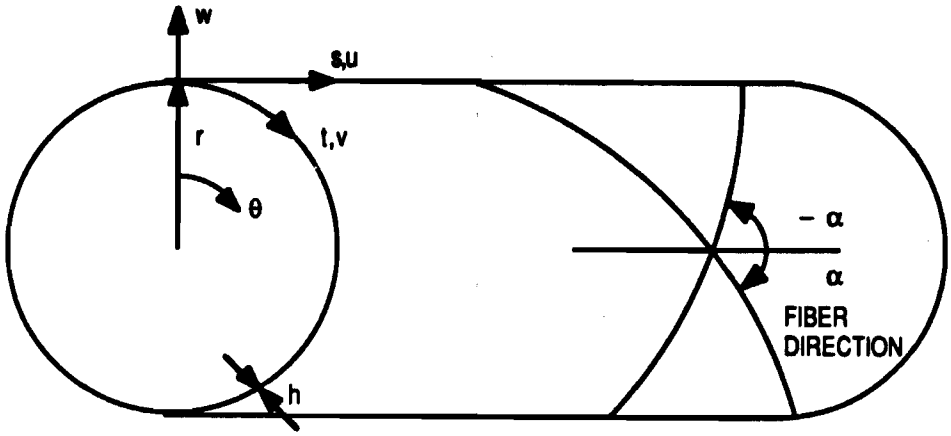

Figure 1: Membrane Cylinder Coordinates, r, s and t, and Displacements, u, v and w.

The equations of equilibrium in a membrane cylindrical shell [6] are defined in the meridianal, circumferential and radial directions, s, θ and r, respectively. These coordinates are indicated on Figure 1. The tangential coordinate t is the same direction as the cirumferential in that $dt = r\ d\theta$. Partial differentiation in the surface of the shell is indicated by the subscripted comma notation. The membrane shell or line force, N, is a force per unit length of shell, and the surface traction, q, is a force per unit area. Employing this nomenclature, the equilibrium equations are as follows:

$$N_{s,s} + N_{s\theta,t} + q_s = 0 \tag{1a}$$

$$N_{s\theta,s} + N_{\theta,t} + q_\theta = 0 \tag{1b}$$

$$\frac{1}{r} N_\theta = q_r \tag{1c}$$

The relations between shell force and mid-surface strain in a membrane orthotropic shell are given below. E, G and ν are axial modulus, shear modulus and Poisson's ratio, respectively, and h is the shell thickness.

$$\epsilon_s = \frac{1}{E_s h}(N_s - \nu_{\theta s} N_\theta) \tag{2a}$$

$$\epsilon_\theta = \frac{1}{E_\theta h}(N_\theta - \nu_{s\theta} N_s) \tag{2b}$$

$$\gamma_{s\theta} = \frac{1}{G_{s\theta} h} N_{s\theta} \tag{2c}$$

One may define membrane shell stiffness terms as follows:

$$C_{ss} \equiv \frac{E_s h}{1 - \nu_{s\theta}\nu_{\theta s}} \tag{3a}$$

$$C_{\theta\theta} \equiv \frac{E_\theta h}{1 - \nu_{s\theta}\nu_{\theta s}} \tag{3b}$$

$$C_{s\theta} \equiv G_{s\theta} h \tag{3c}$$

$$C_{ss\theta\theta} \equiv \nu_{s\theta} C_{\theta\theta} = \nu_{\theta s} C_{ss} \tag{3d}$$

Equation 3d takes advantage of the reciprocity property of orthotropic materials, $\nu_{s\theta}E_\theta = \nu_{\theta s}E_s$. The relations between mid-surface strain and shell force are then found by inverting Equations 2a– 2c, giving:

$$N_s = C_{ss}\epsilon_s + \nu_{s\theta}C_{\theta\theta}\epsilon_\theta \tag{4a}$$

$$N_\theta = C_{\theta\theta}\epsilon_\theta + \nu_{\theta s}C_{ss}\epsilon_s \tag{4b}$$

$$N_{s\theta} = C_{s\theta}\gamma_{s\theta} \tag{4c}$$

The relations between shell mid-surface displacements and membrane strains are as follows:

$$\epsilon_s = u_{,s} \tag{5a}$$

$$\epsilon_\theta = v_{,t} + \frac{w}{r} \tag{5b}$$

$$\gamma_{s\theta} = u_{,t} + v_{,s} \tag{5c}$$

By substituting the strain-displacement relations, 5a–5c, into the force-strain relations, 4a–4c, one can obtain the following force displacement relations:

$$N_s = C_{ss}u_{,s} + \nu_{s\theta}C_{\theta\theta}\left(v_{,t} + \frac{w}{r}\right) \tag{6a}$$

$$N_\theta = C_{\theta\theta}\left(v_{,t} + \frac{w}{r}\right) + \nu_{\theta s}C_{ss}u_{,s} \tag{6b}$$

$$N_{s\theta} = C_{s\theta}\left(u_{,t} + v_{,x}\right) \tag{6c}$$

The membrane cylinder constitutive equations defined above are the basis for the elastically coupled concentric shell derivation. The stiffness properties have been derived assuming homogeneous, orthotropic materials. For a composite shell the moduli would represent equivalent through-the-thickness properties. The derivation of these equivalent properties based on composite shell theory is provided in the following section.

2.2 Orthotropic Shell Stiffness Properties

The membrane stiffness properties of a composite shell in an orthotropic layup are derived here. The overall properties of the shell are obtained by summing the properties of a sequence of individual plies [7]. In the following discussions an $\alpha = 0°$ ply is assumed to align with the meridianal direction of the shell, s. Off-axis plies are assumed to be layed up symmetrically so that there is no axial-shear coupling. Thus for every ply at a non-zero angle α, there is an identical ply at an angle $-\alpha$.

2.2.1 Lamina Properties

Strain-stress relations for an individual lamina are given below in terms of the lamina stiffness coefficients Q. When the ply is aligned with the meridian of a cylindrical shell, the 1 and 2 directions will correspond to the s and t directions, respectively. The stiffness properties reflect a state of plane stress in the lamina.

$$\begin{Bmatrix} \sigma_1 \\ \sigma_2 \\ \tau_{12} \end{Bmatrix} = \begin{bmatrix} Q_{11} & Q_{12} & 0 \\ Q_{12} & Q_{22} & 0 \\ 0 & 0 & Q_{66} \end{bmatrix} \begin{Bmatrix} \epsilon_1 \\ \epsilon_2 \\ \gamma_{12} \end{Bmatrix} \tag{7}$$

$$Q_{11} = \frac{E_1}{1-\nu_{12}\nu_{21}} \tag{8a}$$

$$Q_{22} = \frac{E_2}{1-\nu_{12}\nu_{21}} \tag{8b}$$

$$Q_{12} = \frac{\nu_{12}E_2}{1-\nu_{12}\nu_{21}} = \frac{\nu_{21}E_1}{1-\nu_{12}\nu_{21}} \tag{8c}$$

$$Q_{66} = G_{12} \tag{8d}$$

To be physically realizable, the lamina properties must obey: $|\nu_{12}| < \sqrt{E_1/E_2}$, and $\nu_{12}E_2 = \nu_{21}E_1$.

2.2.2 Laminate Properties for a Symmetric Layup

For a pair of plies lain at angles $\pm\alpha$ to the meridian, the strain-stress relations are:

$$\begin{Bmatrix} \sigma_s \\ \sigma_\theta \\ \sigma_{s\theta} \end{Bmatrix} = \begin{bmatrix} \bar{Q}_{ss} & \bar{Q}_{ss\theta\theta} & 0 \\ \bar{Q}_{ss\theta\theta} & \bar{Q}_{\theta\theta} & 0 \\ 0 & 0 & \bar{Q}_{s\theta} \end{bmatrix} \begin{Bmatrix} \epsilon_s \\ \epsilon_\theta \\ \gamma_{s\theta} \end{Bmatrix} \tag{9}$$

Note that coupling terms between extensional and shear deformations are zero due to the symmetric layup assumption[1]. The lamina stiffness properties are defined as follows, where the shorthand notation $\mathrm{c} = \cos\alpha$ and $\mathrm{s} = \sin\alpha$ has been employed.

$$\bar{Q}_{ss} = Q_{11}\mathrm{c}^4 + Q_{22}\mathrm{s}^4 + 2\left(Q_{12}+2Q_{66}\right)\mathrm{s}^2\mathrm{c}^2 \tag{10a}$$

$$\bar{Q}_{\theta\theta} = Q_{11}\mathrm{s}^4 + Q_{22}\mathrm{c}^4 + 2\left(Q_{12}+2Q_{66}\right)\mathrm{s}^2\mathrm{c}^2 \tag{10b}$$

$$\bar{Q}_{ss\theta\theta} = Q_{12}\left(\mathrm{s}^4+\mathrm{c}^4\right) + \left(Q_{11}+Q_{22}-4Q_{66}\right)\mathrm{s}^2\mathrm{c}^2 \tag{10c}$$

$$\bar{Q}_{s\theta} = Q_{66}\left(\mathrm{s}^4+\mathrm{c}^4\right) + \left(Q_{11}+Q_{22}-2Q_{12}-2Q_{66}\right)\mathrm{s}^2\mathrm{c}^2 \tag{10d}$$

[1] A possible means of damping a tube we have not investigated would be to fabricate concentric tubes, the inner one having all positive ply layup angles and the outer tube having negative angle plies. Axial loads on the tube would generate opposite torsion in the two tubes, and hence shear in the enclosed VEM layer. The ends of the concentric tubes would likely need to be free to rotate independently about the tube axis to obtain maximum damping.

2 CONCENTRIC SHELL FINITE ELEMENT DERIVATION

The total shell thickness is the sum of the lamina thicknesses, $h = \sum h_j$. The total stiffness properties of the laminate C can be obtained by summing the individual lamina properties weighted by their thicknesses. Average moduli, E_s, E_θ and $G_{s\theta}$, and average Poisson's ratio, $\nu_{s\theta}$, may then be derived using the definitions for laminate stiffnesses given in Equations 3a–3d.

$$C_{ss} = \sum \bar{Q}_{ss,} h_j \tag{11a}$$

$$C_{\theta\theta} = \sum \bar{Q}_{\theta\theta,} h_j \tag{11b}$$

$$C_{ss\theta\theta} = \sum \bar{Q}_{ss\theta\theta,} h_j \tag{11c}$$

$$C_{s\theta} = \sum \bar{Q}_{s\theta,} h_j \tag{11d}$$

2.3 Mechanics of the Viscoelastic Layer

Constitutive equations are derived here for the viscoelastic layer constrained between the two concentric elastic shells, which together make up the damped tube finite element. The sandwiching arrangement is shown in Figure 2.

The viscoelastic material (VEM) is assumed to be at a single operating frequency, which allows the elastic and shear moduli, E_V and G_V, to be defined as complex numbers representing magnitude and phase of stiffness. The analysis can be repeated for different operating frequencies and temperatures. It should be emphasized that the analysis presented here is for one temperature and frequency.

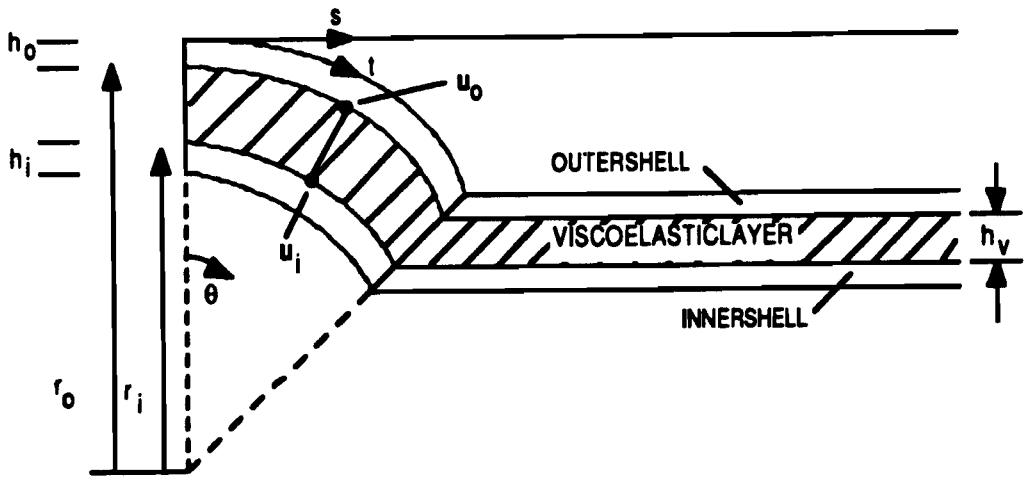

Figure 2: Representation of VEM Sandwiched Between Two Concentric Shells

The derivation is performed first for arbitrary motions in a cylindrical coordinate system, and then specialized to the case of radially symmetric motions.

2.3.1 Viscoelastic Medium Constitutive Relations

The relations between displacement and strain in the VEM are given below [8]. The components of the displacement vector $\mathbf{u}_V$ are in the radial, meridianal and tangential directions, r, s and t, respectively.

$$\epsilon_r = u_{r,r} \tag{12a}$$
$$\epsilon_s = u_{s,s} \tag{12b}$$
$$\epsilon_\theta = u_{\theta,t} + \frac{u_r}{r} \tag{12c}$$
$$\gamma_{\theta s} = u_{\theta,s} + u_{s,t} \tag{12d}$$
$$\gamma_{sr} = u_{r,s} + u_{s,r} \tag{12e}$$
$$\gamma_{\theta r} = u_{\theta,r} + u_{r,t} - \frac{u_\theta}{r} \tag{12f}$$

Relations between strains and stresses in the VEM sandwich layer are:

$$\begin{Bmatrix} \sigma_r \\ \sigma_s \\ \sigma_\theta \end{Bmatrix} = \frac{E_V}{(1+\nu)(1-2\nu)} \begin{bmatrix} 1-\nu & \nu & \nu \\ \nu & 1-\nu & \nu \\ \nu & \nu & 1-\nu \end{bmatrix} \begin{Bmatrix} \epsilon_r \\ \epsilon_s \\ \epsilon_\theta \end{Bmatrix} \tag{13}$$

A modified VEM elasticity term has been defined to simplify subsequent notation: $\tilde{E}_V \equiv \frac{E_V}{(1+\nu)(1-2\nu)}$. The shear stress strain relations are simply:

$$\sigma_{ij} = G_V \gamma_{ij} \quad ; \qquad i \neq j \tag{14}$$

2.3.2 Strains Given Shell Displacements

The displacements within the VEM are assumed to vary linearly in the radial direction between the inner and outer shells. This is felt to be a very good assumption when the VEM layer is thin. In that case, one can largely ignore the change in circumference of the medium in the radial direction. Thus stresses, and hence strains, will be almost uniform through the thickness of the VEM layer, h_V. The VEM displacement vector $\mathbf{u}_V$ is assumed to be related to the displacement vectors of the inner and outer shells, $\mathbf{u}_i$ and $\mathbf{u}_o$ as follows:

$$\begin{aligned} \mathbf{u}_V(s,\theta,r) &= \mathbf{u}_i(s,\theta)\frac{r_o - r}{h_V} + \mathbf{u}_o(s,\theta)\frac{r - r_i}{h_V} \\ &\equiv \mathbf{u}_i(s,\theta)\,R_i(r) + \mathbf{u}_o(s,\theta)\,R_o(r) \end{aligned} \tag{15}$$

The shells have been assumed to be thin enough that the mid-surface displacements are identical to the displacements at the surface in contact with the VEM. In other words, the inner and outer shells have their stiffness properties defined at their outer and inner

surfaces, respectively. For simplicity, the shape functions $R_i(r)$ and $R_o(r)$ have been defined representing radial dependence due to unit displacements of the inner and outer shells, respectively.

Strains in the VEM due to individual components of inner and outer shell displacements are obtained by inserting the displacements defined in Equation 15 into the strain-displacement Equations 12a- 12f.

$$\epsilon_r = \frac{w_o - w_i}{h_V} \tag{16a}$$

$$\epsilon_s = u_{i,s}R_i + u_{o,s}R_o \tag{16b}$$

$$\epsilon_\theta = v_{i,t}R_i + v_{o,t}R_o + \frac{1}{r}[w_iR_i + w_oR_o] \tag{16c}$$

$$\gamma_{rs} = w_{i,s}R_i + w_{o,s}R_o + \frac{u_o - u_i}{h_V} \tag{16d}$$

$$\gamma_{r\theta} = \frac{v_o - v_i}{h_V} + (w_{i,t}R_i + w_{o,t}R_o) - \frac{1}{r}(v_iR_i + v_oR_o) \tag{16e}$$

$$\gamma_{s\theta} = (v_{i,s}R_i + v_{o,s}R_o) + (u_{i,t}R_i + u_{o,t}R_o) \tag{16f}$$

Since the VEM layer is assumed to be very thin, one may assume that strains at the middle of the layer are representative of strains throughout. A correction to the average stresses to allow balance of load transfer between inner and outer shells is derived in the next section. Average extensional and shear strains, $\bar{\epsilon}$ and $\bar{\gamma}$, are evaluated at the average radius, $\bar{r} = \frac{r_i + r_o}{2}$. The radial shape functions, $R_i(\bar{r})$ and $R_o(\bar{r})$, both equal $\frac{1}{2}$ under this assumption. The VEM strains given shell displacements then simplify to:

$$\bar{\epsilon}_r = \frac{w_o - w_i}{h_V} \tag{17a}$$

$$\bar{\epsilon}_s = \frac{1}{2}(u_{i,s} + u_{o,s}) \tag{17b}$$

$$\bar{\epsilon}_\theta = \frac{1}{2}(v_{i,t} + v_{o,t}) + \frac{1}{2\bar{r}}(w_i + w_o) \tag{17c}$$

$$\bar{\gamma}_{rs} = \frac{1}{2}(w_{i,s} + w_{o,s}) + \frac{u_o - u_i}{h_V} \tag{17d}$$

$$\bar{\gamma}_{r\theta} = \frac{v_o - v_o}{h_V} + \frac{1}{2}(w_{i,t} + w_{o,t}) - \frac{1}{2\bar{r}}(v_i + v_o) \tag{17e}$$

$$\bar{\gamma}_{s\theta} = \frac{1}{2}(v_{i,s} + v_{o,s}) + \frac{1}{2}(u_{i,t} + u_{o,t}) \tag{17f}$$

2.4 Coupling Shells to the Viscoelastic Medium

Through surface tractions, the thin viscoelastic layer couples the motion of the inner and outer shells which together compose the damped tube. Given some reasonable assumptions

on the compliance of the VEM its deformations can be made wholly dependent on the shell motions, simplifying analysis considerably. The coupling procedure is explained in this section. It is developed first for arbitrary motions, and then specialized to the case of radial symmetry. Radially symmetric motions include both axial and breathing motions. The axial solution is applicable to bending motions through an analogy similar to that employed in the Bernoulli-Euler hypothesis of beam bending. Solutions for the case of radial antisymmetry (torsion) may be derived along similar lines to the radially symmetric case.

2.4.1 Simplifying Assumptions

The following set of assumptions allow the problem to be simplified considerably. The motion of the viscoelastic material can be made dependent entirely on shell motions, leaving these as the only independent variables.

A. The load carrying capability of the VEM layer in its plane (s-θ) is ignored, i.e. σ_θ, σ_s, and $\sigma_{s\theta}$ are assumed to be zero. If the VEM is considerably softer than the shells this will be valid. Essentially one requires the following:

$$(E_V h_V)\,\epsilon_\theta \ll C^{i+o}_{\theta\theta}\epsilon_\theta \tag{18a}$$

$$(E_V h_V)\,\epsilon_s \ll C^{i+o}_{ss}\epsilon_s \tag{18b}$$

$$(G_V h_V)\,\gamma_{s\theta} \ll C^{i+o}_{s\theta}\gamma_{s\theta} \tag{18c}$$

where the superscript $i+o$ simply means that the stiffness properties of the inner and outer elastic cylinders has been added together.

B. The VEM will act to transfer loads between the two tubes; i.e. $\sigma_r, \sigma_{r\theta}$ and σ_{rs} are non-zero and significant. This will generally be true if the VEM layer is thin.

C. No external surface tractions are applied to the inner or outer shells other than those due to stresses in the VEM layer. Loads are applied only through meridianal and shear forces at the ends of an element, and through reactions due to boundary conditions.

D. The loads transferred between inner tube and outer tube due to the VEM tractions must balance. Specifically this requires that

$$|q_i|r_i\,d\theta\,ds = |q_o|r_o\,d\theta\,ds = (\bar{\sigma}_V \cdot \hat{r})\;\bar{r}\,d\theta\,ds \tag{19}$$

where $\hat{r}$ is the unit vector in the radial direction, $\bar{\sigma}_V$ is the stress tensor in the VEM evaluated at its average radius, and q is a traction vector on an inner or outer shell due to the VEM stress. The tractions applied to the shells will thus be:

$$(q_r, q_s, q_\theta)_i = +(\bar{\sigma}^V_{rr}, \bar{\sigma}^V_{rs}, \bar{\sigma}^V_{r\theta})\frac{\bar{r}}{r_i} \tag{20a}$$

$$(q_r, q_s, q_\theta)_o = -(\bar{\sigma}^V_{rr}, \bar{\sigma}^V_{rs}, \bar{\sigma}^V_{r\theta})\frac{\bar{r}}{r_o} \tag{20b}$$

2.4.2 Specialization to Radial Symmetry

The case of radial symmetry allows many terms to be discarded, This enables the derivation of a semi-analytical finite element based on closed form solutions within the domain between circumferential nodes on the shell. Specifically, one may ignore: all partial derivatives in the circumferential direction, i.e. $\frac{\partial}{\partial t}$; the shell quantities v, q_θ, $\gamma_{s\theta}$, and $N_{s\theta}$; and the VEM quantities $\sigma_{r\theta}$, $\sigma_{s\theta}$ (which is assumed zero in any case).

The VEM tractions on the inner and outer shells defined in Equations 20a and 20b may be inserted into the shell equilibrium equations. The meridianal equilibrium Equation 1a becomes:

$$N^o_{s,s} = +\bar{\sigma}^V_{rs}\left(\frac{\bar{r}}{r_o}\right) \tag{21a}$$

$$N^i_{s,s} = -\bar{\sigma}^V_{rs}\left(\frac{\bar{r}}{r_i}\right) \tag{21b}$$

After multiplying both sides by inner or outer radius, as applicable, the radial equilibrium Equation 1c simplifies to:

$$N^o_\theta = -\bar{r}\bar{\sigma}^V_{rr} \tag{22a}$$

$$N^i_\theta = -\bar{r}\bar{\sigma}^V_{rr} \tag{22b}$$

2.4.3 Elimination of Radial Displacements

These equilibrium equations can be expressed entirely in terms of shell displacements. One must substitute the shell force-displacement Equations 6a and 6b, the VEM average strain-displacement Equations 17a–17e, and the VEM stress-strain Equations 13 and 14. The meridianal equilibrium equations on the outer and inner shells become:

$$C^o_s u^o_{,ss} + (\nu_{s\theta}C_\theta)^o \frac{1}{r_o} w^o_{,s} = +G_V\left[\frac{u^o - u^i}{h_V} + \frac{1}{2}\left(w^o_{,s} + w^i_{,s}\right)\right]\left(\frac{\bar{r}}{r_o}\right) \tag{23a}$$

$$C^i_s u^i_{,ss} + (\nu_{s\theta}C_\theta)^i \frac{1}{r_i} w^i_{,s} = -G_V\left[\frac{u^o - u^i}{h_V} + \frac{1}{2}\left(w^o_{,s} + w^i_{,s}\right)\right]\left(\frac{\bar{r}}{r_i}\right) \tag{23b}$$

The radial equilibrium equations become:

$$C^o_\theta \frac{w^o}{r^o} + (\nu_{\theta s}C_S)^o u^o_{,s} = -\tilde{E}_V\bar{r}\left[\frac{1-\nu}{h_V}\left(w^o - w^i\right) + \frac{\nu}{2}\left(\frac{w^o + w^i}{\bar{r}} + u^o_{,s} + u^i_{,s}\right)\right] \tag{24a}$$

$$C^i_\theta \frac{w^i}{r^i} + (\nu_{\theta s}C_S)^i u^i_{,s} = +\tilde{E}_V\bar{r}\left[\frac{1-\nu}{h_V}\left(w^o - w^i\right) + \frac{\nu}{2}\left(\frac{w^o + w^i}{\bar{r}} + u^o_{,s} + u^i_{,s}\right)\right] \tag{24b}$$

Due to assumption C above, i.e. that no shell tractions exist other than those due to the VEM, the radial equilibrium equations can simply be solved for the radial displacements.

2 CONCENTRIC SHELL FINITE ELEMENT DERIVATION

The displacements w are thus wholly dependent on the meridianal strains $u_{,s}$ in the inner and outer tubes, and may be expressed as follows:

$$w^o = a_{oo}u^o_{,s} + a_{oi}u^i_{,s} \tag{25a}$$
$$w^i = a_{io}u^o_{,s} + a_{ii}u^i_{,s} \tag{25b}$$

The meridianal equilibrium Equations 23a and 23b may now be expressed wholly in terms of the meridianal displacements. Substituting 25a and 25b and collecting terms produces:

$$\left[C^o_s + \left(\frac{\nu_{s\theta}C_\theta}{r}\right)^o a_{oo} - G_{V_o}\left(\frac{a_{oo}+a_{io}}{2}\right)\right]u^o_{,ss} + \left[\left(\frac{\nu_{s\theta}C_\theta}{r}\right)^o a_{oi} - G_{V_o}\left(\frac{a_{oi}+a_{ii}}{2}\right)\right]u^i_{,ss} - \frac{G_{V_o}}{h_V}u^o + \frac{G_{V_o}}{h_V}u^i_{,ss} = 0 \tag{26a}$$

$$\left[\left(\frac{\nu_{s\theta}C_\theta}{r}\right)^i a_{io} - G_{V_i}\left(\frac{a_{oo}+a_{io}}{2}\right)\right]u^o_{,ss} + \left[C^i_s + \left(\frac{\nu_{s\theta}C_\theta}{r}\right)^i a_{ii} + G_{V_i}\left(\frac{a_{oi}+a_{ii}}{2}\right)\right]u^i_{,ss} + \frac{G_{V_i}}{h_V}u^o - \frac{G_{V_i}}{h_V}u^i_{,ss} = 0 \tag{26b}$$

This expression has been compacted by defining weighted VEM shear moduli at the outer and inner shell surfaces: $G_{V_o} \equiv G_V\left(\frac{r}{r_o}\right)$ and $G_{V_i} \equiv G_V\left(\frac{r}{r_i}\right)$.

To simplify further derivations the meridianal equilibrium equations are expressed in the following form:

$$\begin{bmatrix} m_{oo} & m_{oi} \\ m_{io} & m_{ii} \end{bmatrix}\begin{Bmatrix} u^o_{,ss} \\ u^i_{,ss} \end{Bmatrix} + k_V\begin{bmatrix} -\frac{r}{r_o} & \frac{r}{r_o} \\ \frac{r}{r_i} & -\frac{r}{r_i} \end{bmatrix}\begin{Bmatrix} u^o \\ u^i \end{Bmatrix} = \begin{Bmatrix} 0 \\ 0 \end{Bmatrix} \tag{27}$$

Again, for simplicity, a VEM shear stiffness per unit area, $k_V \equiv G_V/h_V$, has been defined.

Equation 27 is a pair of coupled second order differential equations in the meridianal coordinate s. One can assume solutions of the form:

$$\begin{Bmatrix} u^o \\ u^i \end{Bmatrix} = \{\varphi\}\, e^{\alpha s} \tag{28}$$

Insertion into the governing differential equation and solution of the resultant eigenproblem leads to the following eigenvalues:

$$\alpha^2 = 0, \quad \frac{k_V\left[\frac{r}{r_o}(m_{ii}+m_{io}) + \frac{r}{r_i}(m_{oo}+m_{oi})\right]}{m_{oo}m_{ii} - m_{oi}m_{io}} \tag{29}$$

The zero eigenvalue leads to eigenvectors such that $u^o = u^i$. Both rigid body meridianal translations and constant meridianal strains are allowable solutions. Thus for the zero

eigenvalues one obtains the following shape functions in the shell:

$$\left\{ \begin{array}{c} u^o(s) \\ u^i(s) \end{array} \right\} = \left\{ \begin{array}{c} 1 \\ 1 \end{array} \right\} \left(q_1 + q_2 s \right) \tag{30}$$

The non-zero eigenvalues lead to eigenvectors such that

$$u^o = \frac{1 + m_{oi}\frac{\alpha^2}{k_V^o}}{1 - m_{oo}\frac{\alpha^2}{k_V^o}} \cdot u^i \equiv \beta u^i \tag{31}$$

Defining the decay length $\lambda \equiv \sqrt{1/\alpha}$ one obtains the following allowable shape functions in the shell:

$$\left\{ \begin{array}{c} u^i(s) \\ u^o(s) \end{array} \right\} = \left\{ \begin{array}{c} 1 \\ \beta \end{array} \right\} \left(q_3 \cosh \frac{s}{\lambda} + q_4 \sinh \frac{s}{\lambda} \right) \tag{32}$$

The amplitude of the shape functions, q_1 – q_4, remain to be determined. Once they are defined, the entire displacement and stress state can be found. One can assemble the displacements due to the zero and non-zero eigenvalues as follows:

$$\left\{ \begin{array}{c} u^i(s) \\ u^o(s) \end{array} \right\} = \left[\begin{array}{cccc} 1 & 1 & 1 & 1 \\ 1 & 1 & \beta & \beta \end{array} \right] \left\{ \begin{array}{c} q_1 \\ q_2 s \\ q_3 \cosh\left(\frac{s}{\lambda}\right) \\ q_4 \sinh\left(\frac{s}{\lambda}\right) \end{array} \right\} \tag{33}$$

2.5 Element Definition

The preceding derivation has allowed us to solve for the internal displacements and stresses in the concentric shell and VEM layers in closed form. The displacements and stresses are dependent on a set of undetermined shape parameters q. These must be determined through application of boundary conditions to the shells. Figure 3 shows the partition of a shell into one discrete segment of length s_o. The meridianal displacements of the inner and outer shells at the left and right ends, A and B, are the degrees of freedom of the element. These displacement degrees of freedom can be found by evaluating Equation 33 at $s = 0$ and $s = s_o$ for ends A and B, respectively. The elemental displacements are thus:

$$\{u_e\} \equiv \left\{ \begin{array}{c} u_A^i \\ u_A^o \\ u_B^i \\ u_B^o \end{array} \right\} = \left[\begin{array}{cccc} 1 & 0 & 1 & 0 \\ 1 & 0 & \beta & 0 \\ 1 & s_o & \cosh\frac{s_o}{\lambda} & \sinh\frac{s_o}{\lambda} \\ 1 & s_o & \beta\cosh\frac{s_o}{\lambda} & \beta\sinh\frac{s_o}{\lambda} \end{array} \right] \left\{ \begin{array}{c} q_1 \\ q_2 \\ q_3 \\ q_4 \end{array} \right\} \tag{34}$$

2 CONCENTRIC SHELL FINITE ELEMENT DERIVATION

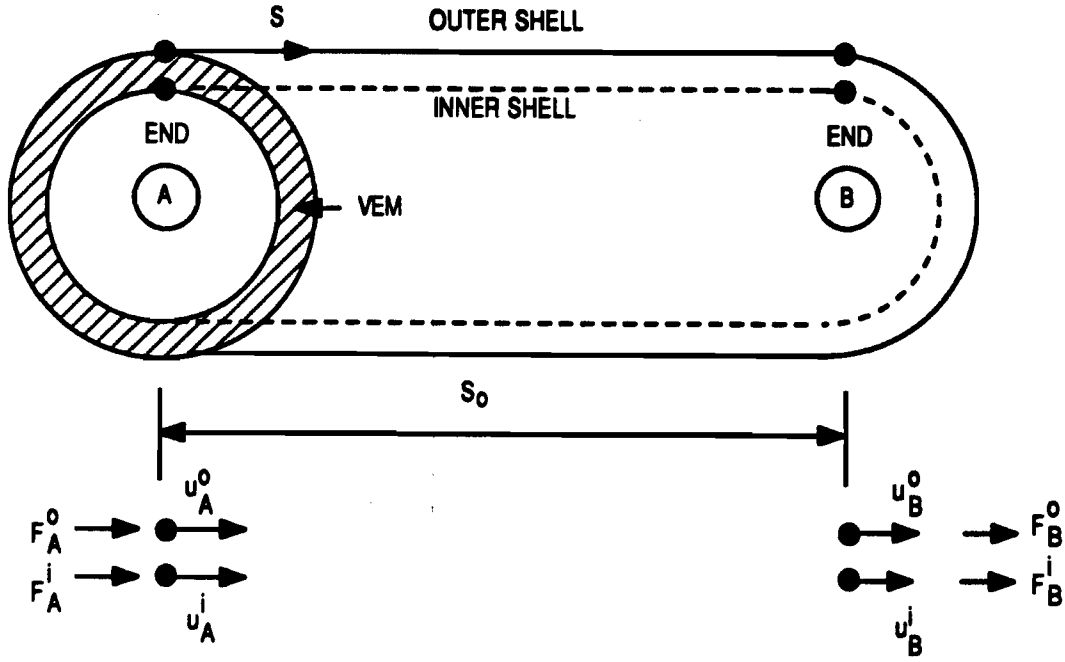

Figure 3: Axial Forces and Displacements on Radially Symmetric Shell Element

With some effort, this expression can be inverted in closed form to give the shape functions q in terms of the element end displacements $\{u_e\}$:

$$\begin{Bmatrix} q_1 \\ q_2 \\ q_3 \\ q_4 \end{Bmatrix} = \frac{1}{1-\beta} \begin{bmatrix} -\beta & 1 & 0 & 0 \\ \frac{\beta}{s_o} & \frac{-1}{s_o} & \frac{-\beta}{s_o} & \frac{-1}{s_o} \\ 1 & -1 & 0 & 0 \\ \frac{-1}{\tanh\frac{s_o}{\lambda}} & \frac{1}{\tanh\frac{s_o}{\lambda}} & \frac{1}{\sinh\frac{s_o}{\lambda}} & \frac{-1}{\sinh\frac{s_o}{\lambda}} \end{bmatrix} \begin{Bmatrix} u_A^i \\ u_A^o \\ u_B^i \\ u_B^o \end{Bmatrix} \tag{35}$$

To obtain a stiffness matrix for the finite element, it is necessary to compute the external forces in terms of the nodal displacements. Starting with Equation 35, one can apply unit displacements to each of the meridianal degrees of freedom of the element $\{u_e\}$ and work backwards through most of the equations of the preceding sections to obtain meridianal shell forces N_s at each end of the shell element. For the case of radial symmetry the only external forces are axial. Radial forces are not allowable due to the membrane shell assumption. The external axial forces are computed from the internal meridianal shell forces by integrating around the circumference to give:

$$\{F_e\} \equiv \begin{Bmatrix} F_A^i \\ F_A^o \\ F_B^i \\ F_B^o \end{Bmatrix} = 2\pi \begin{Bmatrix} r_i N_s^i(0) \\ r_o N_s^o(0) \\ r_i N_s^i(s_o) \\ r_o N_s^o(s_o) \end{Bmatrix} \tag{33c}$$

The element forces thus computed as a function of element displacement allow one to construct an elemental stiffness matrix such that

$$\{F_e\} = [K_e]\{u_e\} \tag{34}$$

2.5.1 Element Assembly

Having an element stiffness matrix, one can construct larger models by mapping a series of elements together end to end. Since this is a one-dimensional element the connectivity is quite simple. Starting at one end of a tube, the axial displacements at the B node of element j are made equal to the displacements at the A end of element $j+1$. A very narrow bandwidth will result, since at most two elements will be connected at any one node. In contrast, the practice of modelling a tube with quadrilateral plates will result in a very large number of elements and a poor bandwidth.

Since the radial displacements w are wholly dependent on the meridianal strains in a membrane shell, and since the stiffness properties can vary from element to element, it is likely that the radial displacements predicted by two adjoining elements will differ. We are enforcing neither radial compatibility nor equilibrium between shell elements. The implications of this are not thought to be major for thin shells, since the behavior we are seeking to model is loading in the stiff in-plane directions. Loads out of plane will generally be orders of magnitude lower. In addition, the bending loads due to radial displacements on a cylindrical shell are known to decay rapidly as one moves away from the point of application in the meridianal direction.

2.5.2 Load Transformation Matrix

In order to simplify stress and load recovery after solution of a load case at a given forcing frequency, internal element response is stored in a load transformation matrix (LTM). This matrix is computed for each element as the elemental stiffness matrix is generated. The matrix gives internal element response $\{L_e\}$ in terms of nodal displacements in the manner:

$$\{L_e\} = [LTM]\{u_e\} \tag{35}$$

The quantities stored in the LTM are: the amplitudes of the element shape functions q; meridianal strains, $u_{,s}$, radial displacements, w, and axial forces, F, at ends A and B of the inner and outer shells; and VEM shear stresses, σ_{rs}, and radial stresses, σ_r at ends A and B. These quantities are generally sufficient to evaluate strength and any other constraints one

might impose during an optimization of the tube properties. The LTM enables one to avoid having to recover internal stresses after problem solution, greatly reducing computation time and programming complexity.

3 Example Problem

A simple example of the use of the code is the uniform segmented constraint. A 324 element Nastran quadrilateral plate model using eight-fold symmetry to reduce complexity, and a one element TUBES model predicted axial stiffness within 1% and loss factor within 4%. The Nastran analysis used the modal strain energy approximation, which accounts for the slightly greater discrepancy in damping predictions.

A difficult problem which can take advantage of the analysis and optimization capabilities of the TUBES program is TRW's Alternating Ply Concept damped tube. A patent application on this approach to integrating passive viscoelastic damping into fiber composite structures was submitted in 1988. The application was filed as "Viscoelastic Damping Structure and Related Manufacturing Method." A tube using this unique ply layup was designed, built and tested at TRW in 1987.

Figure 4 shows cross-sections of damped tubes employing both the uniform segmented constraining layer, which was the best available prior art, and the Alternating Ply Concept, which offers much greater damping levels.

The Alternating Ply Concept tube is essentially two concentric elastic tubes with a VEM layer in between. A large amount of energy can be forced into the VEM through the arrangement of stiff plies lain primarily in a 0° orientation on alternating sides of the VEM layer. These axial plies are short, with some overlap between inner and outer tubes so that load transfer can occur in shear through the VEM. The axial plies are held together by angle plies running continuously along both sides of the VEM layer. The angle plies serve to seal in the VEM. They also prevent the formation of peel stresses since they are in continuous contact with the VEM along the whole length of tube. Lacking fibers in the axial direction, the angle plies are very soft in axial deformation. They thus act as a flexure between the stiff axial plies. The flexing takes place in the gaps between the axial plies. Conversely, the angle plies are stiff in shear and torsion, and so those deformations do not get effectively damped. Axial and bending deformations of the tube can be heavily damped due to the fact that almost all the axial load is forced through the VEM layer.

The Alternating Ply Concept is a blend of series and parallel damper ideas. Design parameters can be shifted to either end of the spectrum between series and parallel. Damping is distributed along the whole length of the tube as in constrained layer damping. High damping levels can be obtained as in joint dampers. The twin parallel elastic load paths through the angle plies provide for static stiffness and strength, and dimensional stability.

3 EXAMPLE PROBLEM

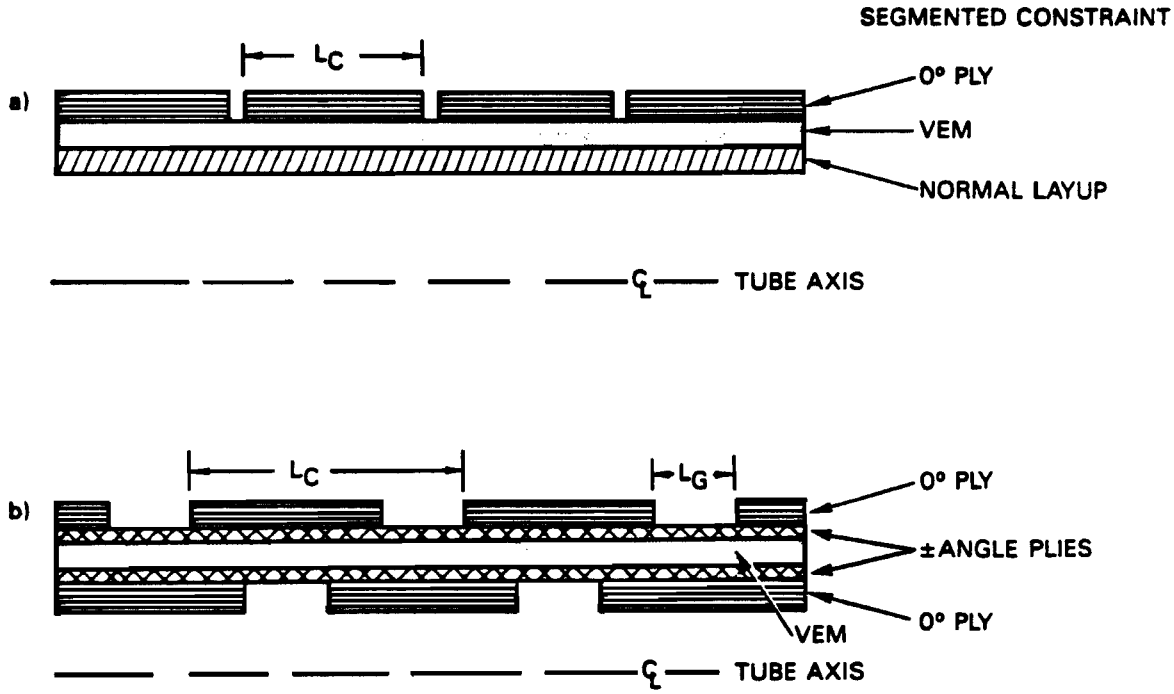

Figure 4: Layup Details and Geometric Design Variables for: a) Uniform Segmented Constaining Layer and b) Alternating Ply Concept.

3.1 TUBES Model

Rather than model a whole tube, the smallest repeatable section, called the unit cell is modeled. This unit cell is shown in Figure 5, along with the element divisions and meridianal displacement degrees of freedom. Note that the model consists of five elements and twelve axial displacement degrees of freedom. The displacements at the left end, u_1 and u_2, are typically constrained to be zero, and the displacements at the right end, u_{11} and u_{12}, are constrained to move together. A unit force is then applied to the right end to determine the complex value of stiffness, from which dynamic stiffness and damping are determined. When inner and outer shell properties are assumed to be the same, the design variables are: t_0, the thickness of the axial plies; t_{45}, the thickness of the angle plies; t_V, the VEM thickness; L_c, the length of the unit cell; and L_g, the length of the gaps between the axial plies. Additionally, one could choose the angle of the angle plies as a design variable, rather than fixing it as we have at 45°.

The properties assumed for the GY-70 angle plies are:
$E_s = 43e6$ psi, $E_\theta = .975e6$ psi, $\nu_{s\theta} = .19$, $\rho = 0.06$ lb/in^3, and $\eta = .002$ (0.1% damping). The properties assumed for the P-100 axial plies are the same as those for the angle plies except the moduli are scaled up by the ratio 74/43. The VEM properties are those for the SQDM-I material for the given operating temperature and frequency. A nomogram for this material, showing shear modulus and loss factor versus reduced frequency, is given in Figure 6. The

3 EXAMPLE PROBLEM

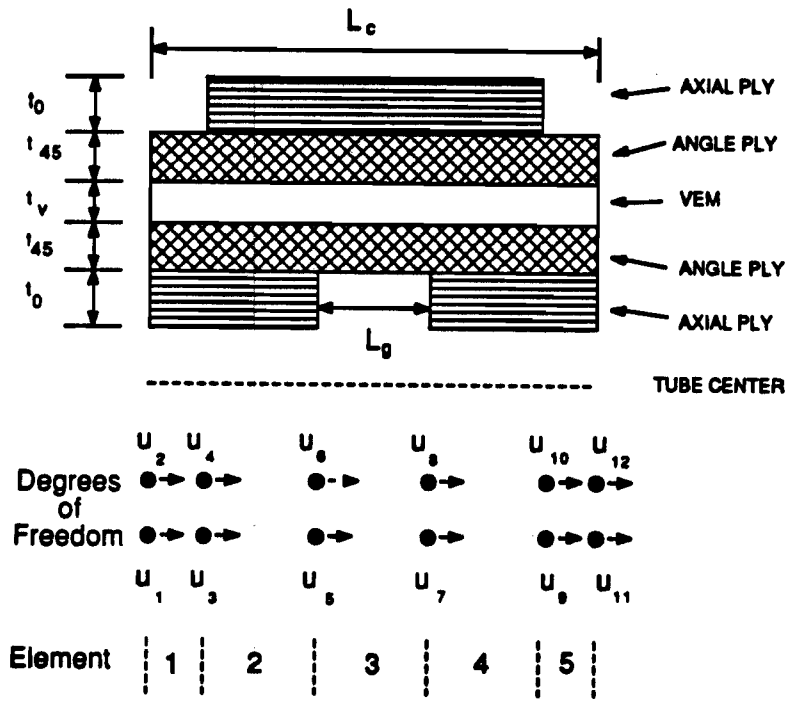

Figure 5: TUBES Model of Unit Cell of Alternating Ply Concept Tube.

VEM thickness was dictated by the available material, and is $t_V = .024$ inches.

A design was optimized to maximize the resonant vibration figure of merit, $FOM^{res} \equiv \frac{E}{\rho}\eta$, which weights loss factor equally with specific modulus. A material concept which maximizes this figure of merit will minimize response at resonance if a structure were fabricated uniformly from the material. A material figure of merit can be defined for a random environment. If one assumed a flat power spectral density and well separated modal frequencies, ω_n, mean square response [9] would be inversely proportional to $\zeta_n\omega_n^3$. A random vibration figure of merit would thus be $FOM_0^{ran} \equiv \frac{E}{\rho}\eta^{2/3}$. In realistic situations the PSD will roll off with frequency. Assuming, as in Reference 10, a $1/\Omega$ roll-off the resultant figure of merit would be $FOM_1^{ran} \equiv \frac{E}{\rho}\sqrt{\eta}$. It turns out that designs optimized for these various figures of merit do not differ greatly. The resonant figure of merit emphasizes damping somewhat more, while the random figures of merit emphasize stiffness somewhat more.

The optimization was performed for VEM properties at room temperature and a frequency of 10 Hertz. The optimized design, after rounding off lengths to the nearest half inch and thicknesses to the nearest available ply thickness, is:
$L_c = 5$, $L_g = 1.5$, $t_{45} = .005$, and $t_0 = .015$, all units in inches.

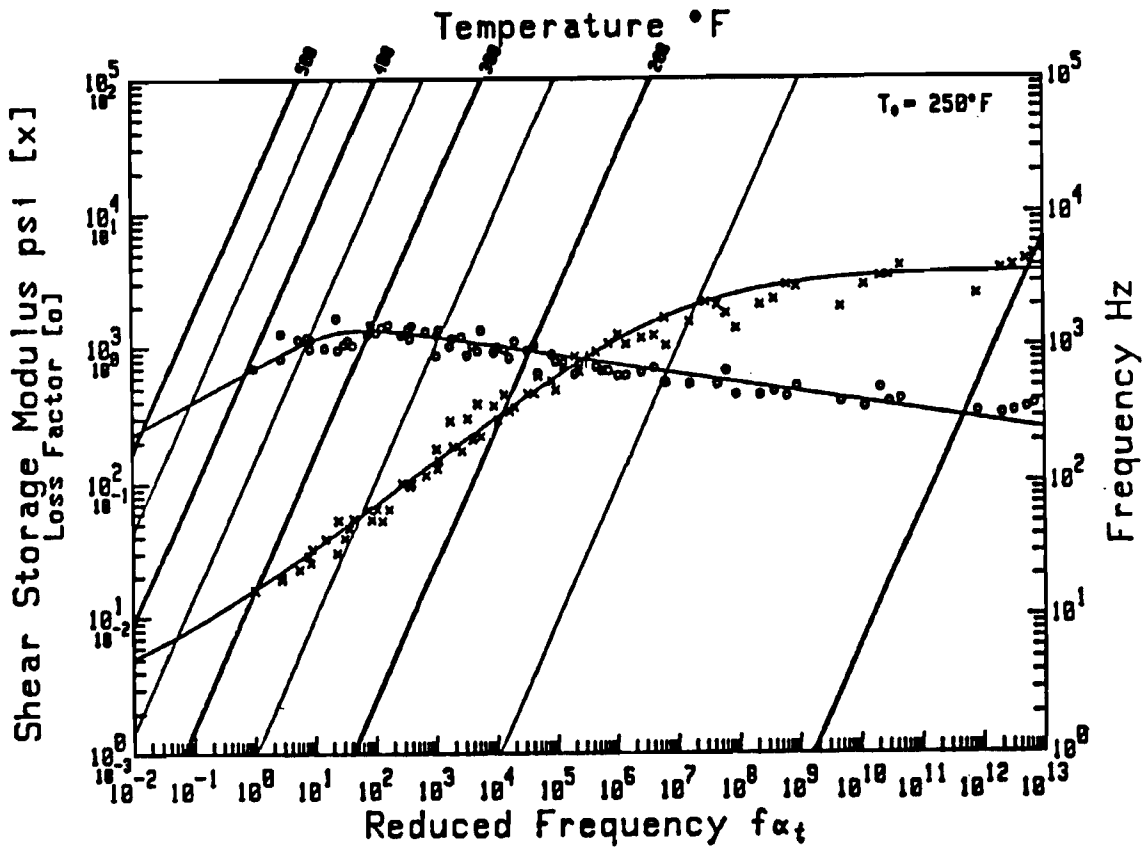

Figure 6: Frequency Nomogram for SQDM-I

3.2 Test Results

Process development tests were first performed to see if the VEM could be cocured into graphite epoxy. A three foot tube, 1.5 inches in diameter was then constructed using the above properties. Free decay vibration tests were performed in cantilever bending. Tip weights were varied to modify frequencies. A blow dryer was used to vary tube temperature. The temperature estimates are thus rather approximate. Six cases were run. The A cases were at room temperature and the B cases were at elevated temperature. Subscripts indicate the number of 4.2 pound tip weights added to the cantilevered tube. Test results are summarized in Table 1, along with analytic results from the TUBES model and VEM properties estimated from the frequency nomogram. Room temperature VEM properties are extrapolations since the curve does not go down low enough in frequency.

Shell stiffness was derived from the bending frequency using the following formulae:

$$EI = Eh\pi R^3$$

3 EXAMPLE PROBLEM

$$f = \frac{1}{2\pi}\sqrt{\frac{3EI}{ML^3}}$$

Given knowledge of the radius, natural frequency and mass, one can back out Eh, which is the effective shell stiffness of the whole layup integrated through the thickness and along one unit cell.

Two sets of damping measurements are given to indicate the difficulty in measuring this parameter when damping is high. Both curve fit and log decrement estimates are given. Natural frequencies are from the curve fit. Correlation of room temperature tests with analysis is not too bad. At elevated temperature, test data indicates that VEM stiffness breaks down more rapidly than the curve fit in the nomogram would indicate. This results in lower shell stiffness. It also is a possible explanation for the lower than predicted damping, since less strain energy will get into the VEM if it is very soft.

Table 1: Damped Tube Test Summary.

			CASE					
			A_0	B_0	A_1	B_1	A_2	B_2
Tip Weight	W	lb	1.07	=	5.27	=	9.47	=
Temperature	T	°F	71	135	71	115	71	120
Natural Frequency	f	Hz	23.4	19.03	9.65	8.50	7.00	5.70
Curve Fit	ζ	%	4.0	8.6	4.8	7.2	6.0	6.4
Log Decrement	ζ	%	3.8	9.0	4.5	6.9	5.3	9.0
Shell Stiffness	Eh	10^5 lb/in	5.4	3.54	4.8	3.7	4.64	3.1
Material Data Estimated from Nomogram								
Reduced Frequency	$f\alpha_t$		?	7E6	1E13	3E8	2E12	4E7
Shear Modulus	G	psi	3800	2000	3500	2600	3400	2200
Loss Factor	η		.2	.6	.25	.49	.28	.55
Analytic Results Using Material Data								
Damping	ζ	%	4.3	12.	5.0	10.	6.0	11.
Shell Stiffness	Eh	10^5 lb/in	5.30	4.00	5.12	4.50	5.05	4.18

3.3 Conclusions

In one of the cases tested, A_1, 43% of the strain energy was absorbed by the VEM. This is phenomenal, and indicates that the use of a VEM with a loss factor of 1 or more would give 43% damping or higher. These high levels of damping can be attained with a structure having a considerable degree of static stiffness. The high damping was sacrificed in our design in order to explore the use of a VEM with reduced temperature dependence. The VEM

was providing a loss factor lower than .3 at room temperature, yet damping between 4 and 6% was obtained.

It is also important to note that the tube was designed in a state of axisymmetric extension, but tested in a state of asymmetric bending. The analysis and test still correlate well. This is because the fibers behave locally like they are in extension even though the tube overall is in bending. Thus the Bernoulli-Euler hypothesis we assumed which allowed axial and bending properties to be equated was verified.

References:

1. J. S. Archer, "Application of New Structural Materials for Spacecraft Design," TRW IR&D project #89330339, January 1987-present.

2. 3M Product Information, Scotchdamp SJ-2015X Type 110, Structural Products Department, St. Paul MN.

3. Plunkett, R. and Lee, C. T., "Length Optimization for Constrained Layer Damping, *Journal of the Acoustical Society of America*, Vol. 48, No. 1, 1970, pp 150-161.

4. Kress, G., "Improving Single-Constrained-Layer Damping Treatment by Sectioning the Constraining Layer," *The Role of Damping in Vibration and Noise Control*, ASME Publication DE-Vol. 5, L. Rogers and J.C. Simonis editors, pp 41-48, presented at ASME 11th Biennial Conference on Vibration, Boston MA, September, 1987.

5. Kuritz, S.P., and Bronowicki, A.J., "Concepts in Integrally Damped Structural Members," presented at ASME 11th Biennial Conference on Vibration.

6. Kraus, H., *Thin Elastic Shells*, Wiley, N. Y., 1967.

7. Jones, R. J., *Mechanics of Composite Materials*, McGraw-Hill, N. Y., 1975.

8. Sechler, E. E., *Elasticity in Engineering*, Dover, N. Y., 1952.

9. Clough, R. W. and Penzien, J., *Dynamics of Structures*, McGraw-Hill, N. Y., 1975.

10. Bronowicki, A. J., "Structural Modification to Minimize Response of Electro-Optical Systems to Random Excitation," in Vol. 748 of the Proceedings of SPIE, *Structural Mechanics of Optical Systems II*, A. E. Hathaway Editor, 1987.